THESIS FOR THE DEGREE OF LICENTIATE OF ENGINEERING

# Quantum Chemical Exploration of Nitriles in Prebiotic Chemistry and Astrobiology

HILDA SANDSTRÖM

Department of Chemistry and Chemical Engineering

CHALMERS UNIVERSITY OF TECHNOLOGY

Gothenburg, Sweden 2020

Quantum Chemical Exploration of Nitriles in Prebiotic Chemistry and Astrobiology

HILDA SANDSTRÖM


Licentiatuppsatser vid Institutionen för kemi och kemiteknik
Chalmers tekniska högskola
Nr 2020:20

Department of Chemistry and Chemical Engineering
Chalmers University of Technology
Chalmersplatsen 4
SE-412 96 Gothenburg
Sweden
Telephone + 46 (0)31-772 1000

Printed by Department of Chemistry and Chemical Engineering
Gothenburg, Sweden 2020

Quantum Chemical Exploration of Nitriles in Prebiotic Chemistry and Astrobiology

HILDA SANDSTRÖM

Department of Chemistry and Chemical Engineering

Chalmers University of Technology

ABSTRACT

The Universe hosts countless different chemical environments, such as planets, moons, comets and the interstellar medium. The diverse pressures, temperatures and chemical compositions of these environments make a wide variety of processes possible. Knowledge about the chemical processes that occur in such remote locations is largely limited by what is observable by telescopes or site-specific missions. Gaining a deeper understanding of this chemistry is valuable when testing different hypotheses regarding the history and evolution of our Universe and can be important for informing the design of space missions.

In this thesis we computationally evaluate the thermodynamic and kinetic stability of chemical structures that may be relevant to prebiotic chemistry, the chemistry that preceded life, and astrobiology. The thesis describes the use of steered molecular dynamics to study the formation of iminoacetonitrile, a hydrogen cyanide dimer and a proposed prebiotic intermediate. The mechanism of iminoacetonitrile formation is found to be consistent with an established hypothesis. However, the reaction is predicted to proceed over a timescale of several months near room temperature, two orders of magnitude slower than the rate of polymer appearance. Future studies into the reactivity of iminoacetonitrile are proposed to better delineate a comparison between theory and experiments.

We investigate the plausibility for a different kind of membrane structure, the azotosome, to form in the frigid hydrocarbon lakes of Titan. Comparisons of the stability of azotosomes relative to the crystal structure of their building block acrylonitrile predict that self-assembly of such membranes is unlikely.

**Keywords:** astrochemistry, metadynamics, hydrogen cyanide, iminoacetonitrile, azotosome, acrylonitrile, Titan

LIST OF PAPERS:

This thesis is based on the work presented in the following papers:

**I.** **The Formation of Iminoacetonitrile, a Missing Prebiotic Intermediate, in Polar Media.** Sandström, Hilda and Rahm, Martin
*Manuscript*

**II.** **Can polarity-inverted membranes self-assemble on Titan?**
Sandström, Hilda and Rahm, Martin.
*Science Advances 6 (2020) eaax0272*

CONTRIBUTION REPORT

Paper I. I performed the quantum chemical calculations and co-wrote the manuscript together with M.R.

Paper II. I performed the quantum chemical calculations and co-wrote the manuscript together with M.R.

LIST OF ABBREVIATIONS

| | |
|---|---|
| DFT | Density functional theory |
| CCSD(T) | Coupled cluster with single-double and perturbative triple excitations |
| PCM | Polarizable continuum model |
| PBE | Perdew–Burke-Ernzerhof |
| B3LYP | Becke, 3-parameter, Lee-Yang-Parr |
| HCN | Hydrogen cyanide |
| HNC | Hydrogen isocyanide |
| DNA | Deoxyribonucleic acid |
| RNA | Ribonucleic acid |
| VASP | Vienna ab initio simulation package |

# Table of Contents

# Chapter 1
# Introduction

In the Universe, and in our solar system, there are extremely diverse environments characterized by their pressure, temperature and chemical composition. Inside planets the pressure can reach large values of hundreds of GPa,[1] while in the interstellar medium, molecules are present in near vacuum.[2] In a similar way, the temperature and radiation density vary between environments.[2] The environmental diversity makes a vast number of chemical reactions possible. Often the diverse conditions are difficult to reproduce without great expense. Some studies of chemical reactions will therefore be out of laboratory reach. Computational chemistry can help in many of these circumstances and enable studies of processes in extreme chemical environments or timescales. For example, simulations using chemical reaction networks can help explain the abundances of chemical species. There is a continuous feedback between observations and models in order to validate our understanding of the ongoing processes. This thesis focuses on applying computational chemistry to evaluate hypotheses in prebiotic chemistry (Paper I) and of astrobiology occurring under cold conditions (Paper II).

In low-temperature environments, chemical processes are different than at room-temperature in a number of ways. The exponential dependence of the rate constant on temperature makes reactions slow due to the small available thermal energy. Under low-temperature conditions competing reactions favour kinetic products, separated from the reactants by the lowest barrier, rather than the thermodynamic products which have the lowest free energy. Under very cold conditions, even weak van der Waals interactions are relatively strong compared to the available thermal energy and many compounds exist in their condensed solid phase. Moreover, the low temperature limits diffusion, among other processes. Examples of astrochemical low-temperature environments include the interstellar medium, comets and asteroids and some planets and moons. These astrochemical environments contain clues about the history of our solar system and our planet.

The branch of chemistry which focuses on the abiotic formation of biologically important molecules is called prebiotic chemistry. One focus of such research is, for example, to explain the creation of life's building blocks in the conditions of the early Earth. Similarly, astrobiology involves research on the origins of life including the possibilities of extra-terrestrial life and its detection characteristics, biosignatures. One largely unanswered question in prebiotic chemistry is how larger organic molecules, macromolecules, can form abiotically, and to which extent they can form under low temperature conditions. Understanding how easily biologically relevant molecules can form under different conditions can provide insight into the uniqueness of life on Earth.

## 1.1 Aim

This thesis has two aims. The first relates to the assumed role of hydrogen cyanide (HCN) polymers in prebiotic chemistry (Paper I). We aim to determine whether a proposed HCN dimerization reaction is consistent with polymerization experiments by evaluating the HCN dimerization energy profile. The second aim relates to the potential of membrane formation in the lakes of Titan (Paper II). We evaluate the likelihood of the formation of a membrane structure, the acrylonitrile azotosome, through thermodynamical arguments.

## 1.2 Chemistry on Titan

One example of an environment where low-temperature chemical processes occur is Saturn's moon Titan. Titan has a thick atmosphere made out of methane and nitrogen.[3] Figure 1.1 shows how photochemistry in the atmosphere leads to the formation of complex organic species.[4] Some of the photochemical products in the atmosphere condense to form aerosols, and some form larger complex organic species.[5] The chemical processes leading to the formation of large organics on Titan are largely unknown.[6]

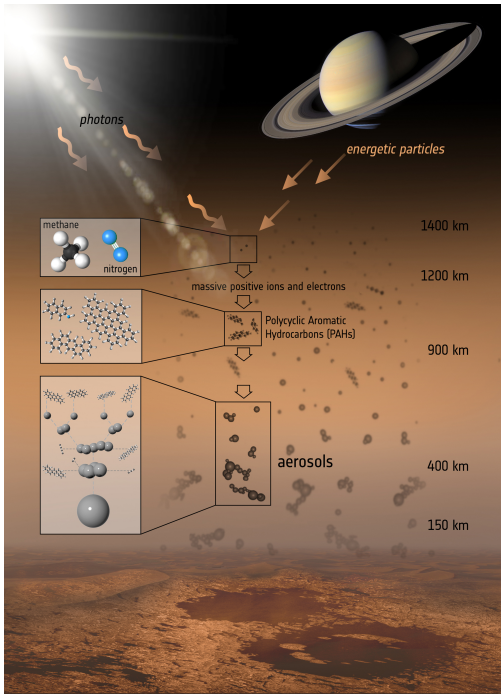


**Figure 1.1.** The formation of Titan's haze. The photochemistry occurring at above 1000 km is connected to the formation of more complex molecules like polyaromatic hydrocarbons, and aerosol particles form at lower altitudes. Image by European Space Agency (ESA).[7]

Many of the organic molecules observed on Titan are also common on Earth. In fact, Titan's atmospheric chemistry is believed to be similar to that of early Earth. For example, methane, nitrogen and ammonia are present and there is no free oxygen.[8, 9] However, in stark contrast to Earth, Titan's atmospheric temperature does not exceed 200 K at any altitude.[10]

At the surface, the temperature is an even colder 94 K.[11] Because of the cold temperature, the surface is covered in organic material that is frozen solid. Beneath the top layer of organic dust, there is frozen water.[12] Energy in the form of sunlight is scarce at the surface, after passing through the upper layers of the thick atmospheric haze.[13] When the possibilities of chemistry driven by photons or thermal energy is limited, chemical processes can be expected to be slow.

In the near future, the Dragonfly mission will be launched equipped with landers that will collect data from dunes and impact craters on the surface.[14] The craters on Titan's surface are remnants of high-energy impacts that momentarily provided the surface with a unique source of energy, and most likely exposed liquid water to the organic material on the surface.[15]

Titan is the only other body in the solar system, other than Earth, which is known to have lakes and seas.[16] There are methane clouds in Titan's atmosphere and a corresponding methane cycle in similarity to the hydrological cycle on Earth.[17] The lakes of Titan mostly consist of methane and ethane,[16] and are completely different in nature compared to water. Hydrocarbons like methane and ethane are hydrophobic rather than hydrophilic, meaning that anything that could dissolve in Titan's lakes would behave in a very different manner compared to how it would in an aqueous environment. After the two space missions, Voyager 1 and Cassini-Huygens, there is still much that is unknown regarding the rich chemistry of Titan.

## 1.3 Theoretical Chemistry as a Tool for Astrochemistry

One of the challenges in understanding the chemistry occurring in an environment like Titan is the fact that the temperature and timescales to consider are so different. When evaluating plausible chemical pathways and chemical stability, the following aspects are central: thermodynamics and kinetics. With theoretical chemistry methods, the energy of reactants, products, and transition states can be obtained (see Chapter 2). The difference in free energy of the reactants and products determines whether the reaction will be spontaneous, in accordance with the second law of thermodynamics. At low temperatures, the entropic contribution to the free energy is smaller than at higher temperatures. Therefore, intuition about the spontaneity of a reaction at room-temperature needs to be modified for lower temperatures. The same applies for the kinetics of a reaction, which depends on the difference in energy between a transition state and reactants - the activation energy. If the activation energy is high relative to the thermal energy, $k_B T$, the rate constant for a thermally driven reaction will be small. Figure 1.2 shows how the first-order half-life for a reaction depends on the activation energy at different temperatures. A reaction with a half-life of 1 year at the surface of Titan (~100 K) requires a barrier of 70 kJ/mol less than one in ambient conditions on Earth. An energy of 70 kJ/mol is approximately equivalent to the strength of Adenine base-pairing (Figure 1.2).

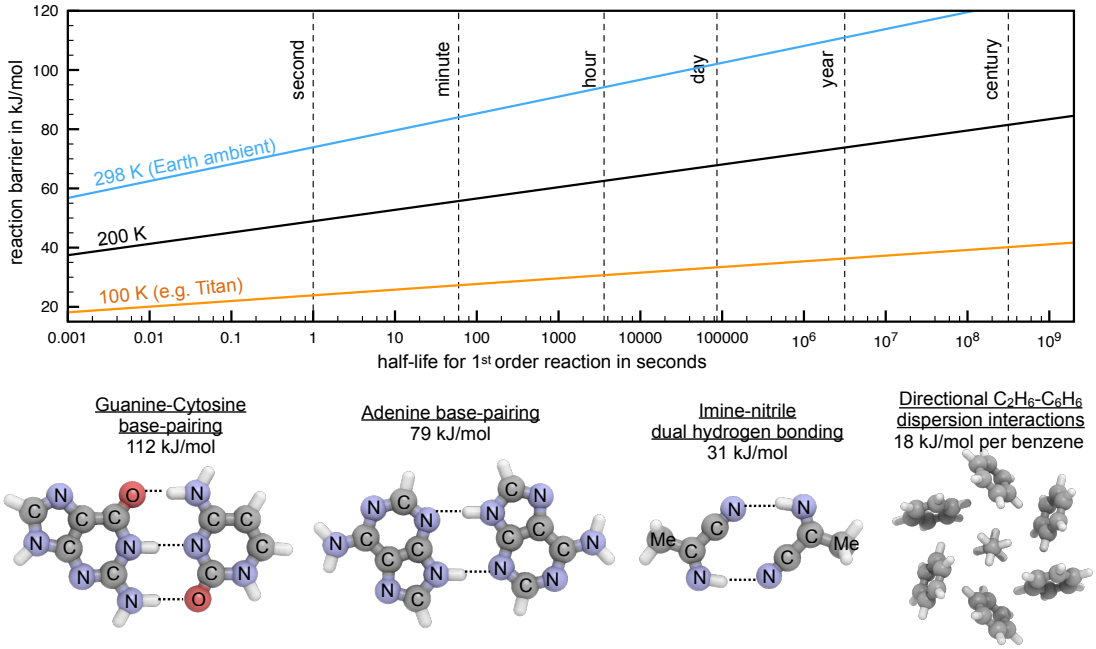


**Figure 1.2. Top:** Reaction energy barriers required for chemical processes to occur over ms to century timescales in different environments (rate estimates via transition-state theory). **Bottom:** Examples of structure-directing secondary interaction with varying strength. Stacked guanine-cytosine base pairs are strong enough to maintain the DNA double helix on Earth, but far too strong to allow thermally driven dynamical processes under colder conditions. The figure is adapted with permission from reference (18).

# Chapter 2
# Quantum Chemistry Methods

There are a number of approaches for calculating free energies of chemical structures using theoretical chemistry methods. The content of this chapter serves as a reference when we present and discuss Papers I and II for which methods presented herein were used.

The presentation benefits from a partition of the contributions to the free energy, $G$, as a sum of the electronic energy, $\mathrm{E_{el}}$ , and thermal corrections, $\mathrm{E_{thermal}}$ according to

$$G = E_{el} + E_{thermal}. \tag{2.1}$$

The electronic energy is a result of the interactions between the electrons and atomic nuclei and can be found by solving the Schrödinger equation. The thermal corrections have both enthalpic and entropic contributions that are temperature dependent (see Section 2.3).

## 2.1 Quantum Chemical Approaches to Obtaining the Electronic Energy

The electronic energy $E_{el}$ can be found by solving the time-independent Schrödinger equation

$$\mathrm{H}\Psi = E_{el}\Psi, \tag{2.2}$$

where $\mathrm{H}$ is the Hamiltonian operator, and $\Psi$ is the molecular wave function. Though there exist many different approaches for finding the electronic energy, the most commonly used methods all share some approximations. An important one is the Born-Oppenheimer approximation, in which the electrons are assumed to be moving in a configuration of frozen nuclei.[19] This approximation can be used due to the fact that the nuclei are much heavier than the electrons and therefore move more slowly. Using the Born-Oppenheimer approximation, the wavefunction for the electrons can be found from a Hamiltonian that only considers the kinetic energy and interactions of the electrons. To obtain the wavefunction and energy of the electrons, the energy is minimized by way of the variational principle. The total electronic energy can be found by adding the nuclear-nuclear repulsions, $V_{N-N}$, to the electron energy, $E_e$, (the kinetic energy of the nuclei is later considered in the thermal corrections from the translational degrees of freedom)

$$E_{el} = E_e + V_{N-N}. \tag{2.3}$$

In this thesis we have used two different methods for obtaining the electron energy, density functional theory (DFT), and coupled cluster theory (e.g. CCSD(T)).[20] What follows is a short introduction to DFT. For a description of CCSD(T) we refer to reference (20).

### 2.1.1 A Brief Description of Density Functional Theory

DFT is a successful quantum mechanical method for obtaining the electronic energy because it combines accuracy and speed. The theory was developed based on two key publications by Hohenberg and Kohn[21], and Kohn and Sham[22]. The Hohenberg-Kohn theorem states that given an interparticle interaction, it is possible to formulate the electron energy as a functional of the electron density. This reduces the computational cost compared to an orbital formulation. However, the exact appearance of the functional is unknown. In particular, the kinetic energy and interactions between electrons is challenging. A solution to the question of how to model the kinetic energy was addressed by Kohn-Sham.[22] The electrons are modelled as non-interacting particles moving in an effective potential. The functional formulation of the energy, $E_e[\rho]$, in terms of the electron density, $\rho$, is

$$E_e[\rho] = T[\rho] + \int d^3r\rho(\boldsymbol{r})V_{ext}(\boldsymbol{r}) + \frac{1}{2}\int d^3r\rho(\boldsymbol{r})\, V_H(\boldsymbol{r}) + E_{xc}[\rho], \tag{2.4}$$

where $\boldsymbol{r}$ is a positional vector. The first term in Equation (2.4) corresponds to the kinetic energy, $T[\rho]$ which is calculated for non-interacting electrons (using an orbital formulation). The effective potential functional corresponds to the three other terms: contribution to the energy from interactions between nuclei and electrons represented by the external potential, $V_{ext}$; electrostatic electron-electron interactions represented by the Hartree potential, $V_H$; and the exchange-correlation functional, $E_{xc}[\rho]$.

The exact form of the exchange-correlation functional is unknown. Exchange-correlation accounts for electron-electron interactions beyond the mean-field approximation as well as the error introduced by using a kinetic energy for non-interacting particles. Different rungs of DFT exist which approach the modelling of exchange-correlation in different ways. The most common ones used are generalized gradient approximation DFT[23] and hybrid DFT.[24] In the generalized gradient approximation, the exchange-correlation potential is evaluated based on the electron density and its gradient.[23] Hybrid DFT improves on the accuracy of the generalized gradient approximation by including some of the exchange interactions from Hartree-Fock theory,[24] and is more computationally demanding.

### 2.1.2 Density Functional Theory in Molecular Systems

The electron density, $\rho$, of a molecule can be represented as the sum of the square of the wavefunctions of individual electrons, $\psi_j$, as

$$\rho \;=\; \sum_j \left|\psi_j\right|^2. \tag{2.5}$$

In molecular quantum chemistry software, the wavefunction of an electron in a molecule is often represented by a linear combination of atomic orbitals. Typically, an atomic valence electron orbital is also represented by a linear combination of contracted basis functions, $\phi_i$,

$$\psi_j \;=\; \sum_i c_{ji}\phi_i \tag{2.6}$$

with coefficients, $c_{ji}$. The contracted basis functions are in turn linear combinations of so called primitive gaussian functions. There are a number of existing basis sets which differ in their form (number of basis functions, number of primitive functions) and for what systems they were optimized. Additionally, diffuse and polarized functions can be added to improve the form and flexibility of the basis set. To reduce the computational cost, the core electrons are often assumed to have a frozen description.

### 2.1.3 Density Functional Theory in Periodic Systems

Because of crystal periodicity, the electron density in an entire crystal can be described by the electron density of one unit-cell. In periodic systems, the wave functions of the electrons are often represented as plane waves according to the Bloch theorem. The periodicity of the plane waves making up the electron density is described by their wave vectors **k**. **k** corresponds to a vector in the reciprocal space (i.e. the Fourier transform) of the crystal lattice. The wave function of an electron is described as

$$\psi_j = \sum_k c_{jk} e^{-i\mathbf{k}\cdot\mathbf{r}} \tag{2.7}$$

where $c_{jk}$ is a coefficient and **r** is a positional vector in the crystal lattice. In analogy with the frozen core-description used with gaussian basis sets, one can use pseudopotentials[25] or projected augmented waves[26] in periodic DFT. The objective is similarly to reduce the number of plane waves needed to describe the system accurately. In addition, a cut-off for the highest kinetic energy of the electrons is used to control the size of the basis set.

The energy of a crystal depends on long-range interactions. It is computationally favourable to consider these interactions in reciprocal space. Evaluating the energy in reciprocal space requires integration over different values of **k**. These are evaluated as sums in periodic DFT software. The sums in turn are evaluated on a *k*-point grid. If the function varies a lot in reciprocal space, a fine grid is needed for an accurate description. If the function varies little, sampling a few *k*-points is enough. It is necessary to converge both number of *k*-points and energy cut-off in order to obtain accurate energies and forces.

## 2.2 Molecular and Material Geometry Optimizations

The relative energy of different chemical states is found by comparing the most stable geometries of those states. To this end we perform geometry optimizations on the multidimensional potential energy surface. The reactants and products correspond to minima on the potential energy surface (Figure 2.1). The transition state, on the other hand, is a first-order saddle-point, or maxima (in a one-dimensional potential energy surface). A minimum or saddle-point can be classified by inspection of the vibrational frequencies.

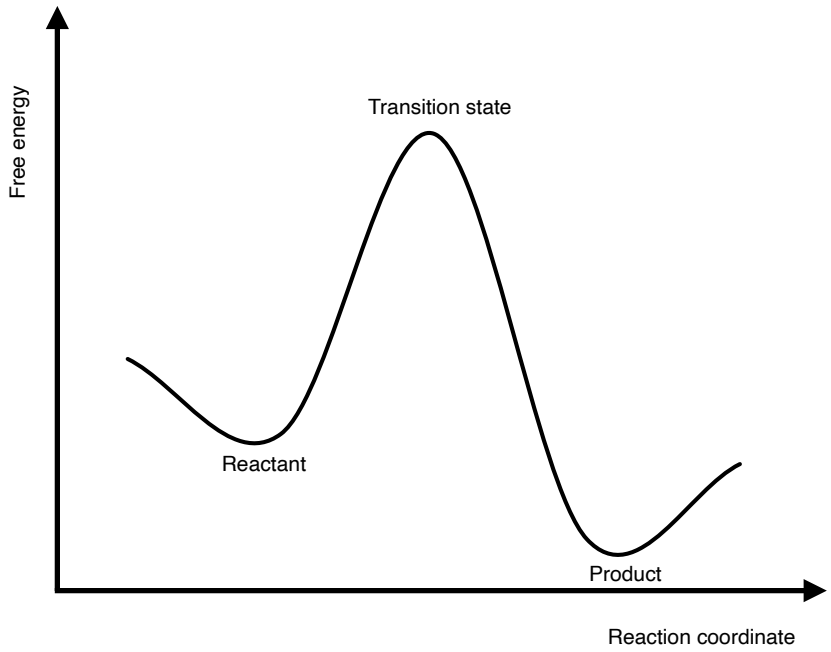


**Figure 2.1** Schematic of an energy profile of a reaction, visualized in one dimension. The reactant and product correspond to minima on the potential energy surface. In a general number of n-dimensions, the transition state is a first-order saddle-point (a minimum in all coordinates but one for which it is a maximum).

## 2.3 Calculating Thermal Effects in Molecules and Solids

In all systems, the thermal effects included in $E_{thermal}$, depend on how the molecule or material can store energy in its rotational, vibrational or translational degrees of freedom as well as on the associated entropy. The total thermal correction is

$$E_{thermal} = E_{vibration} + E_{rotation} + E_{translation}, \quad (2.8)$$

where $E_i$ is the thermal energy contribution for degree of freedom *i*. $E_i$ depends on both an enthalpic contribution, $H_i$, and entropic contribution, $S_i$, according to

$$E_i = H_i - TS_i. \quad (2.9)$$

where $T$ is the temperature. Both the enthalpic and entropic contributions can be calculated from the partition function for the rotational, vibrational and translational degrees of freedom. For example, the vibrational contribution to the thermal correction is obtained by first calculating the force constant of each normal mode of vibration. The force constants are then used to form the total vibrational partition function. An additional contribution to the thermal corrections from the electronic partition function is added if the molecule has a degenerate electronic ground state.

In solids, thermal corrections to the energy are computed only from the vibrational degrees of freedom, called phonons. In this thesis, phonon frequencies were obtained through the finite displacement method. [27] The method involves evaluating the forces associated with displacements of the atoms in the structure.

## 2.4 Modelling Solvent Effects

In a solvated system, there are many possible and complex solvent configurations. Because of the complexity and often large system sizes required to describe a solvent, treating solvent interactions explicitly is challenging. A simpler and common computational approach is to describe interaction with a solvent implicitly, using, for instance, a polarizable continuum model (PCM).[28] In PCM, the solvent molecules are replaced by an average continuum with some dielectric constant. With this method it is not possible model specific interactions with the solvent such as hydrogen bonding.

## 2.5 Molecular Dynamics Simulations

Molecular dynamics simulations are simulations of the time-evolution of a molecular system. In Born-Oppenheimer dynamics (used in this thesis),[29] the energy and the forces which accelerate the system are calculated with DFT, which is described in previous sections. The system is evolved according Newton's equations of motion in discrete steps. An accurate integration in Born-Oppenheimer molecular dynamics requires the time step to be smaller than the fastest movement in the system,[30] often on the order of femtoseconds.

The temperature in a simulation is controlled using a thermostat which modulates the velocities of the atoms, for example by rescaling the velocities. The canonical sampling through velocity rescaling[31] thermostat, which is used in this work, introduces noise to the equations of motion to produce a canonical ensemble.

### 2.5.1 Sampling the Free Energy Landscape Using Steered Molecular Dynamics

There are a number of methods, other than the one described in Section 2.3, through which one can obtain the free energy of a chemical process. Two of them are called metadynamics and umbrella sampling. Both methods are variants of steered molecular dynamics and both have been used in the work leading up to this thesis. One advantage of using steered molecular dynamics methods to obtain free energies is that they are statistics-based methods, as opposed to methods relying on optimizations. Calculations of vibrational frequencies are computationally expensive. Steered molecular dynamics methods are therefore suitable when investigating reaction barriers in large systems. Another advantage of using molecular dynamics is the ability to model a reaction in a solvent modelled explicitly. Umbrella sampling and metadynamics are methods designed to increase sampling of high energy (i.e. unlikely) regions of the potential energy landscape. Simulations are computationally demanding, and without steering the simulation, it would not be possible to gather enough statistics of the high energy regions.

### 2.5.2 Metadynamics

Metadynamics is a suitable method to use when the reactivity of a system is of interest.[32] In metadynamics, exploration of different regions of a configurational space is encouraged by adding a bias potential to the position of the system at regular intervals. This means that as the metadynamics simulation progresses, the potential energy landscape becomes more and more flat, since the likelihood of adding bias to low energy regions is higher than to high energy regions. As the difference in relative energy between regions shrinks, more areas of the configurational space are sampled. The free energy landscape is retrieved as the inverse of the total added potential bias. In that sense, performing metadynamics simulations is like making a cast out of the potential energy landscape. The time-evolution of a deposited bias is visualised in Figure 2.2. We see that after many time-steps, the deposited bias is flat corresponding to a filled landscape. It is possible to locate minima and transition states on the converged surface. The transition state in a simulation can also be identified through committor analysis.[34] A transition state is then defined as a structure from which there is an equal probability of reaching the reactant or product basins.

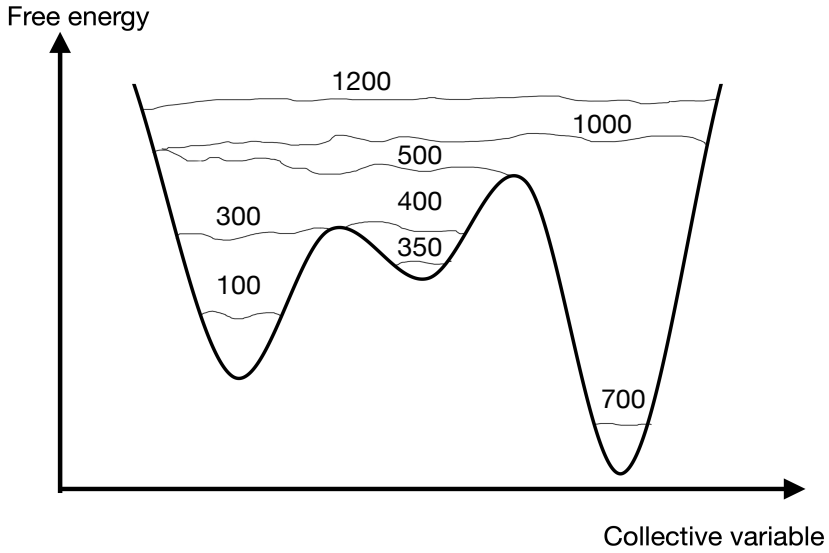


**Figure 2.2** Schematic of snapshots of the deposited bias potential in a metadynamics simulation. The potential free energy landscape is successively filled with deposited bias. Starting from the basin to the left, the system gradually explores states of higher energy until it ends up in another basin. The lines in the diagram represent snapshots of the bias at different times (numbers above line) during the simulation.

Metadynamics requires a set of collective variables that describe the reaction coordinate. As a tool for reactivity exploration, metadynamics can become powerful when combined with path collective variables.[32, 35] There are two path collective variables, $s$ and $z$. The former coordinate describes the position along a reaction path and the latter movement orthogonal to the path. The path collective variables can be constructed using only information of the coordination patterns of structures between which one is interested in finding reaction paths.[36] In contrast to umbrella sampling, which is described next, metadynamics does not force the system to move along the reaction coordinate, but instead allows it to stray to orthogonal paths. Metadynamics is therefore suitable when searching for solvent catalyzed mechanisms.

### 2.5.3 Umbrella Sampling

One of the largest issues with metadynamics is that it can take a long time to converge the free energy landscape. Using umbrella sampling[37] to obtain the energy profile of an observed reaction can be more time efficient. Umbrella sampling is a method in which the chemical system under study is simulated along some reaction coordinate. The free energy, $\Delta G$, is found from the probability distribution, $p(r)$, obtained through the simulation. $p(r)$ describes the relative probability of finding the system at some value of the reaction coordinate, $r$. The free energy is then calculated as

$$\Delta G(r) = -k_B T \ln p(r) \tag{2.10}$$

where $k_B$ is Boltzmann's constant and $T$ is the temperature. In umbrella sampling, a biased probability distribution is obtained instead of $p(r)$. Sampling in high-energy regions of phase space is ensured by constraining the system along the reaction coordinate, $r$, at certain points, $r_0$, with a harmonic bias potential, $V(r)$, on the form

$$V(r) = k(r - r_0)^2, \tag{2.11}$$

where $k$ is a force constant. The gathered biased statistics is then processed to retrieve the relative energy along the sampled reaction coordinate. The accuracy of the retrieved energy profile depends on the sampling. Limited sampling causes an inaccuracy of the energies that can be estimated from so-called block-averaging.[38] Block-averaging is a statistical method based on dividing the total sample into blocks from which the energy profile is calculated. The variation of the energy profile is then used to estimate the error of the profile.

# Chapter 3
# Hydrogen Cyanide and Its Role in Astrochemistry

In this and the subsequent chapter we explore hydrogen cyanide (HCN) chemistry in the context of astrochemistry and prebiotic chemistry. As one of the more common small organic molecules, HCN has been detected on planets,[39–42] comets,[43] Saturn's moon Titan,[44] and in the interstellar medium.[45] Figure 3.1 shows three of those drastically different environments hosting HCN. In the interstellar medium, the HCN can form photochemically from various carbon, nitrogen and hydrogen-containing molecules.[46] In molecular clouds, HCN is found on average at a relative abundance of $10^{-8}$ compared to molecular hydrogen (Panel A, Figure 3.1).[45] The isomer hydrogen isocyanide, HNC, is found at a similar abundance in the interstellar medium despite being 14.8 kcal/mol higher in energy.[47] The reason for the latter is because of a high barrier of isomerization, which impedes conversion from HNC to HCN at low temperatures.[48] In the atmosphere of Titan (Panel B in Figure 3.1), HCN forms as a photochemical product of nitrogen and methane.[49] The volume mixing ratio of HCN increases from $10^{-8}$ at the surface to $10^{-6}$ at 250-300 km altitude.[50] In addition, both the Voyager Flyby and the Cassini mission detected HCN-based aerosol clouds in the atmosphere.[51–53] HCN chemistry in these environments is recognizably difficult to observe directly, or to even emulate experimentally. Moreover, HCN is a hazardous chemical –it can inhibit oxygen uptake by binding to the protein cytochrome C oxidase[54] – and requires careful handling. Because HCN is both volatile and toxic, HCN chemistry is not something easily studied in the laboratory.

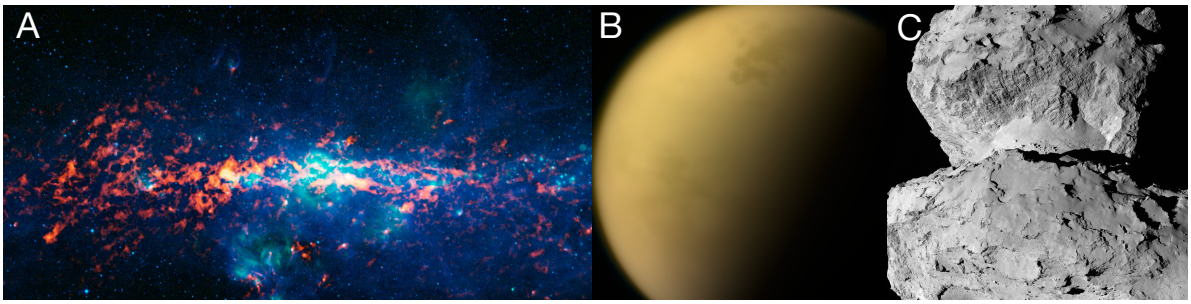


**Figure 3.1.** Examples of three different astrochemical environments where HCN is found. A. The molecular cloud Sagittarus B2 (Image: European Space Observatory(ESO) and NASA)[55] B. Saturn's moon Titan. (Image: NASA/Jet Propulsion Laboratory-Caltech, Space Science Institute)[56] C. The comet 67P/Churyumov-Gerasimenko photographed by the navigational camera onboard Rosetta (Image: European Space Agency (ESA)).[57]

## 3.1 Chemical Properties of HCN

HCN (Figure 3.2a) is an exotic substance in many ways. Under standard conditions, HCN is a volatile liquid with a boiling point close to room temperature (26 °C). Theoretical simulations of the liquid have shown that the HCN molecule is on average coordinated to 7 other monomers in the first solvation shell.[58] HCN has a dielectric constant of 144.8 at 278 K, the sixth largest reported after a group of amides.[59] Experimental gas phase studies of HCN have found that it can form small linear clusters (shown in Figure 3.2c) in the gas phase.[60] Similarly, theoretical studies show that in a hydrogen bonded chain of HCN molecules, the dipole moment increases by a factor of 1.4.[61] Loew et al.[62] found HCN to be anomalous when they correlated the LUMO energy of small nitriles to the Taft σ* substituent coefficients, suggesting that HCN would be less reactive than other nitriles. With a pKa of 9.2, HCN has the historical name prussic acid. HCN is liquid only in a 30 K interval due to its strong intermolecular hydrogen bonds. When it freezes it forms a crystal with a polar unit cell, seen in Figure 3.2b.[63] Anhydrous HCN can be synthesized in different ways, such as by reacting an alkali salt (e.g. potassium or sodium cyanide) with stearic acid, followed by fractional condensation.[64]

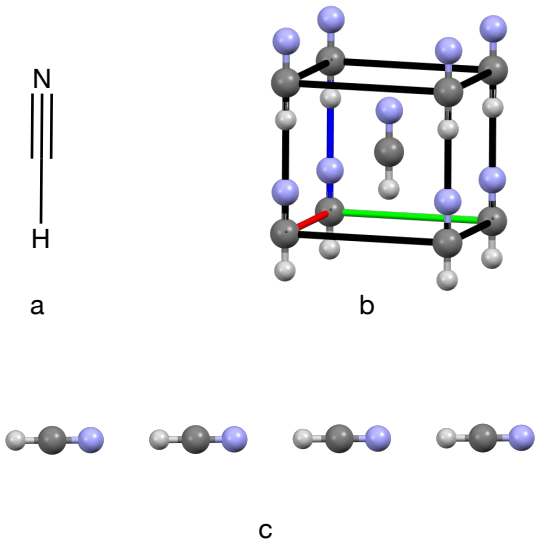


**Figure 3.2**. (a) The Lewis structure of HCN; (b) The conventional unit cell of crystalline HCN;[63] (c) example of a linear cluster of HCN molecules.

## 3.2 HCN in Prebiotic Chemistry

Interest in HCN in the context of prebiotic chemistry began with the famous experiments by Urey and Miller in 1953.[65, 66] In their seminal experiments using electric discharges, adenine (shown in Figure 3.3) formed from simple gas mixtures meant to imitate the atmosphere of early Earth. The proposed prebiotic formation route to adenine included HCN as an intermediate. Later, in 1961 Orò [67, 68] demonstrated that base-catalysed reactions of aqueous HCN indeed can lead to the formation of adenine, along with a host of other compounds. Since the first experiment by Orò, all natural nucleobases of deoxyribonucleic acid (DNA) and ribonucleic acid (RNA) have been identified as products in HCN reaction mixtures (see e.g. reference (69) ) The formation of adenine has been studied and observed in temperatures as low as 195 K.[70] The observation suggests that adenine formation can occur in various cold astrochemical environments. HCN has also been used in prebiotic synthesis of amino acid and ribonucleotide precursors and lipid building blocks.[71]

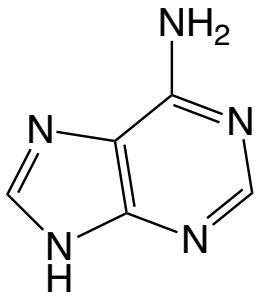


**Adenine**

**Figure 3.3.** The Lewis structure of adenine, one of the nucleobases of DNA and RNA. Adenine is also a pentamer of HCN.

## 3.3 HCN Polymers: How Do They Form and Where?

The relevance of HCN for prebiotic synthesis of biomolecules has motivated the study of HCN reactivity and in particular HCN polymerization. HCN polymerizes under a wide variety of conditions to a complex reaction mixture that often contains a large fraction of insoluble materials (see e.g. reference (72)). Polymerization can proceed both in aqueous phase and in pure HCN. [73] [74] When polymerization experiments are conducted in aqueous solution, the oxygen content has been measured to be between 10 and 25 mole percent.[73, 75, 76, 77] The most favourable pH for HCN polymerization in aqueous solution is 9.2, at the pKa of HCN.[74] Amines or ammonia are typically used as base catalysts.[73, 78] Ferris et al. have also reported that the formation of the HCN tetramer diaminomaleonitrile is catalysed by bromine, iodine, copper ions, cyanogen and cyanamide, and that polymer formation is catalysed by presence of diaminomaleonitrile.[74] Mamajanov and Herzfeld have demonstrated catalysis of HCN polymerization using free radicals[73] and Mozhaev et al. have performed radiation induced polymerization.[79]

The structural possibilities for HCN polymers are many. Because of the ubiquity and reactivity of HCN, HCN polymers and related compounds are suspected to contribute to complex organic matter in a range of environments. For example, macromolecular materials derived from HCN may explain some complex organic matter observed in Titan's atmosphere and on its surface.[80–83]

Several studies have focused on characterization of HCN polymerization products using a variety of techniques such as vibrational spectroscopy, nuclear magnetic resonance spectroscopy and mass spectrometry. The characterization reveals that HCN polymers include a variety of functional groups, such as amines,[76, 76, 84] amides[76, 85], hydroxyl groups,[76], imines, [73, 86] carbodiimides, triazines, nitriles, carbonyls[75] to name a few. Different researchers have proposed different polymer structures based on the results of characterization studies. Three such polymer examples are shown in Figure 3.3. Structure a in Figure 3.3 was proposed by Völker.[77, 84] Meanwhile, Mamajanov and Herzfeld[87] found that new bonds were formed between carbons and nitrogens and proposed structure b in Figure 3.3, in agreement with the irradiation induced polymers of Mozhaev et al.[79]. On the other hand, He et al. found that new bonds were formed between carbons and proposed polyimine (structure c in Figure 3.3).[86] Rahm et al.[85] later showed computationally that polyimine has a tunable band gap which would allow the polymer to absorb visible light in the narrow window of wavelengths that reaches the surface of Titan.

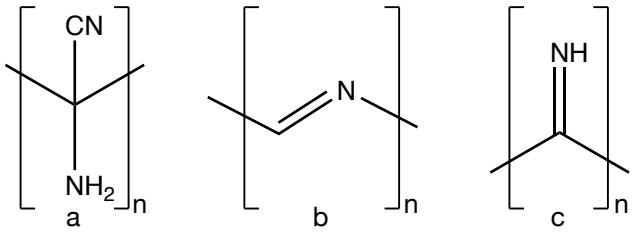


**Figure 3.4**. Three different repeating units proposed for the HCN polymers. a. The ladder-like structure proposed by Völker. [77] b. Head-to-tail polymer by Mozhaev et al.[79] and Mamajanov and Herzfeld [87]c. Polyimine.[86]

The reactive nature of HCN brings about the question: At how low temperatures can HCN polymers form and over what timescale? Answering this question would provide strong hints as to in which different astrochemical environments HCN polymers may be present. So far, the range of temperatures where HCN polymer formation has been observed is between 195-373 K. [73, 78, 88] In aqueous solution, polymerization occurs at concentrations above 0.01 M.[74] At lower concentrations, hydrolysis is the governing process. In cold temperatures, eutectic phases are one way to spontaneously concentrate HCN, favouring polymerization over hydrolysis.[89] In experiments performed close to 250 K, there has been reports of tetramer formation albeit not polymer formation.[72] In one low temperature experiment at 195 K, a 0.15 M HCN 0.1 M ammoniacal solution was left to react and formed polymers over a period of 27 years.[70] Studies of the kinetics of polymerization have also shown that the mechanism appears to change with temperature.[76]

## 3.4 The Mechanism Hypothesis for HCN Oligomerization

In the previous section, we described how HCN polymerization results in a variety of structures, which at least in part depends on reaction conditions. It is naturally unlikely that a single reaction mechanism can account for all such structures. However, before structures diverge it is likely that any HCN polymerization first proceeds through the formation of some kind of dimer. Iminoacetonitrile (Figure 3.5, structure I) constitutes one such dimer and has been proposed to form in the first reaction step of HCN polymer formation. In Paper I we begin to explore the mechanism of HCN polymerization by first explaining the formation of iminoacetonitrile. To understand why we focus on a particular reaction, some context is required.

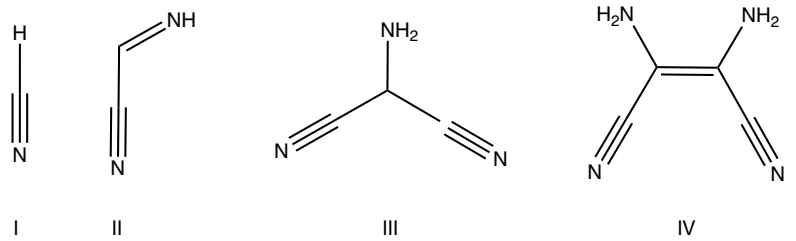


**Figure 3.5**. Four molecules all proposed as intermediates in HCN polymerization: HCN (I), iminoacetonitrile (II), aminomaleonitrile (III) and diaminomaleonitrile (IV).

The early work on HCN reactions by Ferris and Orò identified a number of small molecules as intermediates to adenine and HCN polymers.[68, 90] Figure 3.5 shows the four first intermediates in one of the proposed reaction pathways in HCN polymerization. All four structures correspond to the most stable aliphatic dimer (II), trimer (III) and tetramer (IV). Neither the dimer nor trimer have been detected in polymerization experiments. A likely reason why is that the equilibrium is shifted significantly towards the tetramer or polymer product.[90] The tetramer, or structure IV, is one of the main structures produced in HCN reaction experiments. The confirmed presence of IV in reaction mixtures has given it a central role in most discussions on polymerization pathways. We here note, however, that whereas diaminomaleonitrile is a possible feedstock molecule for the production of polymers, separate polymerization experiments starting from the tetramer do not proceed close to room temperature, like HCN polymerization does.[73, 78]

One mechanism hypothesis involves the successive addition of cyanide anions onto the oligomer since most studied polymers form under alkaline conditions.[68, 90] This mechanism is exemplified in Figure 3.6 for the formation of iminoacetonitrile. The formation of the trimer or diaminomaleonitrile can be imagined in the subsequent steps, first with nucleophilic attacks of CN- on the $sp^2$ carbon of iminoacetonitrile, and then continuing on the formed nitrile group of the trimer. The next chapter describes the thermodynamics and kinetics of iminoacetonitrile formation shown in Figure 3.6.

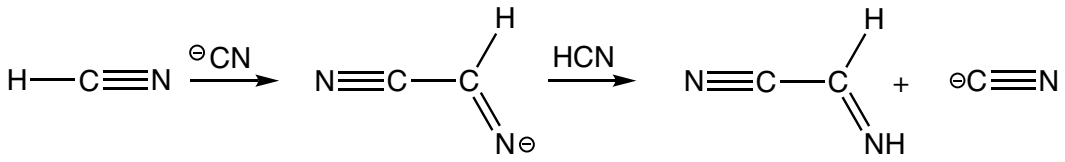


**Figure 3.6.** Proposed formation of iminoacetonitrile through a base-catalyzed mechanism where protonation[68, 90] follows nucleophilic additions of a cyanide anion.

# Chapter 4
# Revisiting Iminoacetonitrile Formation

Our exploration of HCN polymerization mechanisms begins with a closer examination of HCN dimerization in Paper I. The HCN dimer iminoacetonitrile is the hypothesized first intermediate in HCN polymerization. Sanchez et al.[74, 90] have reported that an iminoacetonitrile intermediate was indicated by their kinetics studies of HCN polymerization. However, iminoacetonitrile has never been isolated in polymerization experiments. Structurally related N-alkyliminoacetontiriles have been shown to form maleonitrile derivatives, similar to the often-observed tetramer diaminomaleonitrile.[91]

Claims that iminoacetonitrile should be the HCN dimer that forms in polymerization experiments are motivated by the molecule's relative stability compared to other dimers.[92] An hypothesis of HCN forming a biradical dimer have also been put forth.[79, 87, 93] However, theoretical studies have found iminoacetonitrile to be more stable than the biradical dimer by 26 kcal/mol.[92] Iminoacetonitrile was recently discovered in two molecular clouds, in Sagittarus B2(N) and G + 0.693, adding to the astrochemical interest of the molecule.[94, 95]

Paper I focuses on examining the thermodynamics and kinetics of iminoacetonitrile formation. Despite the fact that most polymerization experiments are performed in either an aqueous or pure HCN environment, only one other theoretical study has focused on iminoacetonitrile formation in a polar environment previously.[96] The method used to describe the solvent was then an implicit solvent model, and the focus was on catalyzation through ion-pairs. In addition, thermal effects were not included. We decided to investigate the formation of iminoacetonitrile in an explicitly described pure HCN environment.

## 4.1 The Formation of Iminoacetonitrile, a Missing Prebiotic Intermediate, in Polar Media

We initially performed metadynamics simulations of a cyanide anion solvated in HCN. These steered simulations were carried out in a canonical ensemble at 278 K. Committor analysis and umbrella sampling were performed to obtain a free energy profile for the reaction that was identified. To this end, we used the path-collective variables, $s$ and $z$, to describe the position along the path between reactants and products, and the position away from the path, respectively (see Paper I). All simulations were performed with the Perdew–Burke-Ernzerhof (PBE)[23] functional and Grimme's D3 dispersion corrections[97] (see Paper I) with Born Oppenheimer molecular dynamics in CP2K v6.1.[98]

After 10 ps of our metadynamics simulation we observed a direct transition from the cyanide anion to iminoacetonitrile with the participation of two HCN molecules. Figure 4.1 shows representative samples of the critical points along the reaction pathway. The carbon-carbon bond is predicted to form simultaneously as a proton transfer occurs between the two HCN molecules. After the transfer, the participating cyanide anion regenerates. The reaction we predict proceeds to the *E*-form of iminoacetonitrile. According to our molecular calculations, the *E*-form is slightly (~1 kcal/mol) more stable in a polar media, while the *Z*-form is slightly more stable in gas phase (<1 kcal/mol).

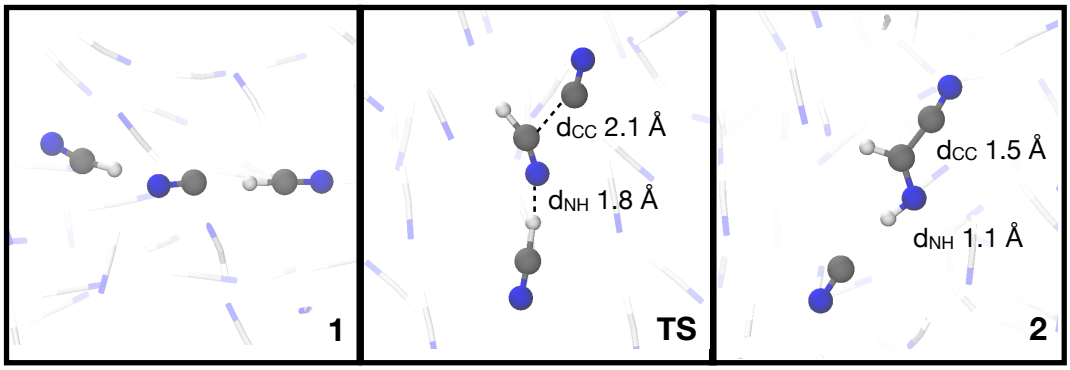


**Figure 4.1.** Formation of *E*-iminoacetonitrile as predicted by a metadynamics simulation of liquid HCN. The mechanism is concerted and involves carbon – carbon bond formation occurring simultaneously with a proton transfer between two HCN molecules.

Figure 4.2 shows the free energy profile of iminoacetonitrile formation as a function of the $s$- and $\zeta$-coordinates. The reaction energy was retrieved through umbrella sampling steered along the $s$-coordinate. At the level of theory used in the simulations, the barrier for iminoacetonitrile formation is 15.5±1.2 kcal/mol and the reaction is exergonic by -7.1±0.8 kcal/mol. The reported uncertainty stems from the limited sampling during the simulations and was estimated through block-averaging.

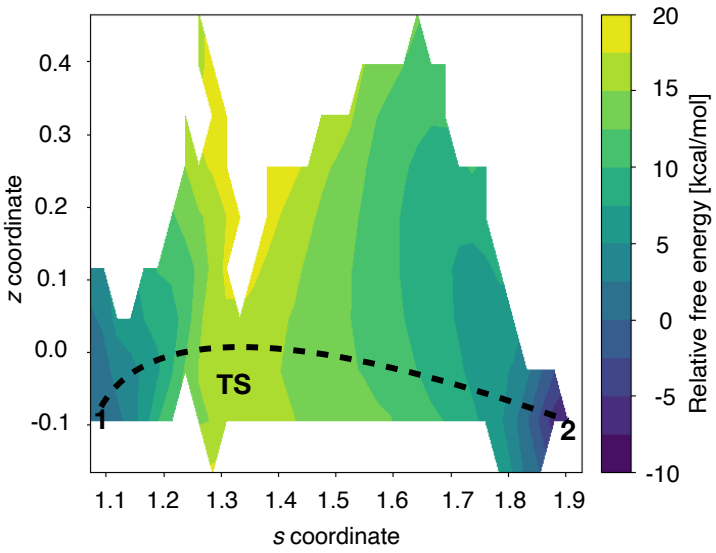


**Figure 4.2.** The free energy landscape of iminoacetonitrile formation in path collective variable space. **1** represents the position of the reactant complex, **TS** the position of the transition state and **2**, the product complex. The white area corresponds to regions not sufficiently sampled during simulations.

Before comparing with experiments, we have added an electronic energy correction, $\Delta E_{corr}$, to our reaction profile, $\Delta G_{US}$. The corrected energy, $\Delta G_{corr}$, was calculated as

$$\Delta G_{corr} = \Delta G_{US} + \Delta E_{corr}, \quad (4.1)$$

where $\Delta E_{corr}$ includes a correction to a higher level of theory and to a larger basis set (for a detailed description, see Paper I). Since it is unfeasible to perform highly accurate single points on our large systems, we based the higher-level calculation on a minimal molecular model containing just the reacting molecules. The HCN solvent molecules were then instead modeled implicitly by a polarizable continuum (see Paper I). After the correction to the electronic energy, the formation of iminoacetonitrile in HCN liquid is only slightly exergonic at 278 K by -0.8±0.8 kcal/mol. The corresponding best estimate for the activation energy is 27.2±1.2 kcal/mol. This is about 11 kcal/mol larger than the apparent polymerization barrier measured by Mas et al. (measured between 323-363 K).[76] The relatively high dimerization barrier is in agreement with dimerization being the rate limiting step for HCN-polymerization.[90]

## 4.2 Estimating the Timescale of Iminoacetonitrile Formation

The timescale of iminoacetonitrile formation in pure HCN can be approximated by calculating the half-life of the reaction using a first order Eyring equation. Figure 4.3 shows the predicted half-life as a function of temperature. We predict that the half-life for the reaction in pure HCN at 278 K is on the order of several months. For comparison, in the studies of Mamajanov and Herzfeld the appearance of polymer (in pure HCN and 278 K) happened on the order of days.[87] He et al. observed a similar experimental polymerization rate in pure HCN at room temperature.[86] The difference between a half-life of days and years at ambient temperature is large, but does not correspond to a large difference in activation energy ( ~3 kcal/mol). One caveat with the comparison of our results to experiments is that our model describes a pure HCN system. Trace amounts of impurities may exist under experimental conditions, facilitating initiation of polymerization. Our model does not either describe the role of known polymerization catalysts, such as ammonia.

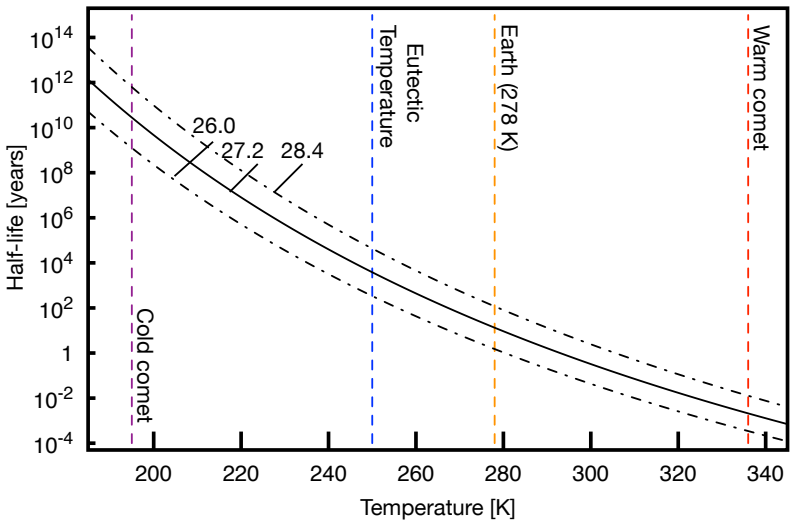


**Figure 4.3.** Our estimate of the half-life for iminoacetonitrile formation as a function of temperature for a solution in pure HCN. The three lines correspond to our barrier estimate 27.2±1.2 kcal/mol. We have here used the barrier calculated at 278 K to extrapolate to lower and higher temperatures. The half-life at the temperature of the simulations (278 K) is on the order of years. Closer to room temperature (300 K) the predicted half-life is within months. At the eutectic temperate, the half-life is thousands of years.

The experimental polymerization rate in aqueous solution (1 M ammonium cyanide, pKa 9.2) is similar to the rates in pure HCN close to room temperature. Assuming the same kinetics for the reaction in water as in HCN allows us to compare our results to experiments performed in a wider range of temperatures. Our predicted timescale for the reaction close to 250 K is on the order of thousands of years. This prediction is not in line with Ferris' observation of tetramer production at such low temperatures after a few days.[74] Rather, it is consistent with the lack of appearance of polymer products in the experiments by Bermejo et al.[72]

If we assume that the effect of the polar liquid environment is similar to a polar frozen one, we can extrapolate our results below the eutectic point, the stoichiometry (74.5 mole percent HCN[89]) and temperature at which the mixture of water and HCN is frozen. After extrapolation, we see in Figure 4.3 that our results cannot explain the appearance of polymer under very cold conditions (195 K) like those formed within 30 years in the experiments of Miyakawa et al.[88] Our calculations predict the considered reaction to proceed on a timescale of billions of years at 195 K (Figure 4.3).

## 4.3 Comparison with Dimerization in an Implicit Solvent

This study was the first of its kind to treat the formation of iminoacetonitrile in explicit solvent. For comparison, we calculated the relative energies of the reactants (**1**), transition state (**TS**) and products (**2**) in implicit solvent as well. The results are presented in Figure 4.4. We used the PCM model for water and exchanged the dielectric constant to that of HCN at 278 K (144.8). With PCM, the barrier for iminoacetonitrile formation was 28.8 kcal/mol in HCN. This is 1.6 kcal/mol higher than the corresponding barrier in the explicit model (Figure 4.4).

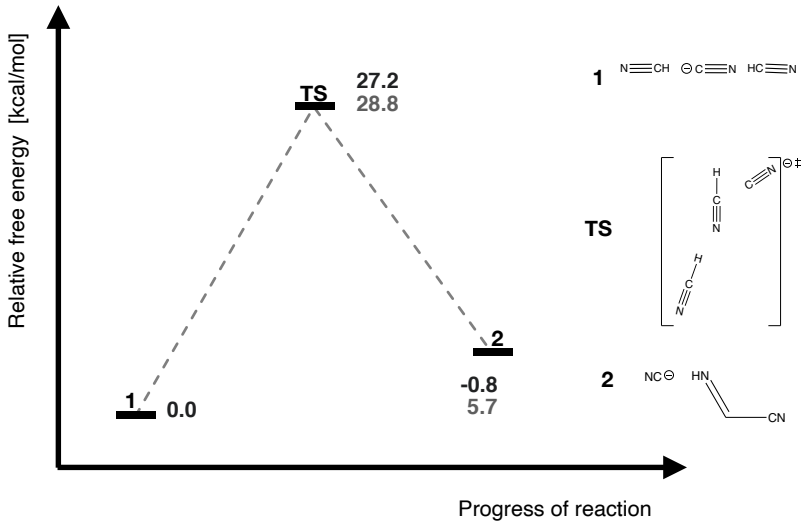


**Figure 4.4**. The corrected free energy profile of iminoacetonitrile formation in HCN modelled in explicit solvent (black) and in PCM (grey). The Lewis structures corresponding to the reactant (**1**), transition state (**TS**) and product (**2**) are shown to the right.

One clear difference between using explicit and implicit solvent descriptions is that PCM shows the reaction to be endergonic. In our explicit solvent model (the simulations) the reaction to iminoacetonitrile appears to be close to thermoneutral. Possible causes for the difference (>5 kcal/mol) between the solvation methods is that PCM either underestimates the stability of the solvated product or overestimates the stability of the reactant. However, we also note that an endergonic reaction does not provide evidence against the dimer forming as a high energy polymerization intermediate. Iminoacetonitrile has yet to be isolated in experiments and must therefore be very reactive if it forms during the polymerization.

Kikuchi et al.[96] previously found that including a hydrogen bonding ammonia in the transition state could lower the activation energy (to 28.7 kcal/mol). We note that our models predict a similar barrier height with HCN acting as the hydrogen bond donor. The effective solvation of ions in polar media like water and HCN disfavors ion-pair formation if the ion concentrations are not very high. In aqueous ammonium cyanide solutions typically used in experiments, the concentration of ammonium is the same as that of cyanide. Both mechanisms are therefore as viable in the typical aqueous solution (1 M and pH 9.2) of ammonium cyanide. However, in pure HCN, coordination by a cation is less likely given the weight percentages of base that are typically used.[86, 87]

## 4.4 Conclusions

To conclude, we have for the first time estimated the reaction energy of iminoacetonitrile computationally, while explicitly considering the effect of the surrounding solvent. The hypothesis of iminoacetonitrile formation under base-catalyzed conditions is supported by its formation in our simulation. However, the predicted dimerization rate is slow compared to the polymerization timescale typically found in experiments. The mechanism is kinetically feasible (i.e. is predicted to occur over a timescale of several months) under typical experimental conditions. However, iminoacetonitrile formation in a polar media is very slow around the eutectic point with water. The conditions on Titan are predicted to be too cold to allow for iminoacetonitrile formation through this pathway. Thermal shocks provided by impacts which momentarily heat up the surface could allow for polymerization to occur, such as the polymerization observed by Mozhaev er al. upon melting solid HCN that had been irradiated at low temperature.[79]

# Chapter 5
# Evaluating the Potential for Cell Membranes in the Lakes of Titan

Membranes are a presumed prerequisite of life as we know it and function so to contain, concentrate and protect the biochemical machinery of cells.[99] All biological membranes known to us exist in an aqueous environment, and most often near Earth ambient conditions. Life on Titan would occur under completely different conditions than on Earth. For example, suggestions of lifeforms able to perform methanogenic metabolism in the hydrocarbon world of Titan[100, 101] challenge our notions of the nature and limits of life. In Paper II, we ask the question of whether unconventional membranes might form and operate under the drastically different conditions of Titan's methane seas.

A membrane in water has a hydrophobic interior and a hydrophilic exterior surface that is exposed to water, as shown in the left panel of Figure 5.1. In water, the driving force which promotes membrane self-assembly is the hydrophobic effect, which maximizes the possible interactions and orientations of the hydrogen bonded water network.[102] This principle would not work in the hydrocarbon seas of Titan which are made up of nonpolar liquids that cannot form hydrogen bonds.

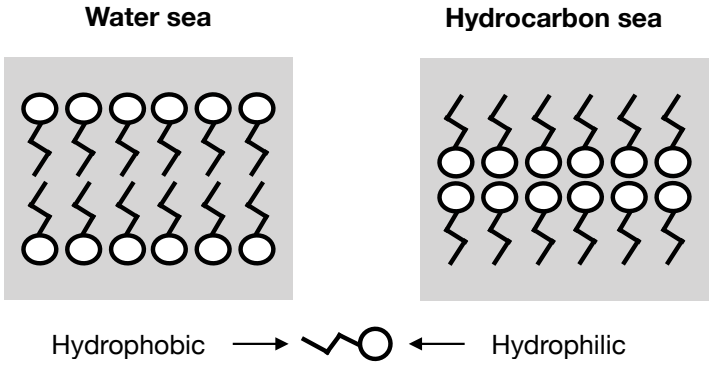


**Figure 5.1** Two ways of arranging molecules into a bilayer membrane. (Left) In water, cell membranes are formed from lipids with hydrophilic ends facing the solvent and hydrophobic parts hidden in the interior of the membrane. (Right) In a hydrocarbon solvent, like methane in the seas of Titan, polar molecules might arrange in a reversed fashion with hydrophilic ends hidden inside the membrane.

In the hydrocarbon sea of Titan, an amphiphilic molecule in a membrane will orient in the opposite way as it would in water, forming an inverted membrane (Figure 5.1). The driving force for membrane self-assembly would also be different. The primary driving force for a hypothetical membrane assembly in a hydrocarbon solvent would be based on a maximization of interactions between the polar ends of the amphiphilic molecules. Such interactions cannot be too strong however, as that would cause a membrane to be too rigid. Since the temperatures on Titan are so low, only small polar molecules would have weak enough intermolecular interactions.

One kind of inverted membranes suggested to form in the hydrocarbon seas of Titan are the azotosomes.[103] Azotosomes are defined as inverted membranes made from polar nitrogen-containing compounds. Out of a number of small amphiphilic molecules, Stevenson et al. computationally showed a promising kinetic viability in azotosomes made from acrylonitrile. Acrylonitrile membranes were also predicted based on calculations to have a flexibility similar to that of membranes on Earth.[103] Following the initial azotosome study, acrylonitrile, the building block of the hypothesized membranes, was detected in the atmosphere of Titan.[104] The detection of acrylonitrile further fuelled interest in the potential existence of azotosomes. The purpose of our work has been to complement the previous study by providing quantum chemical estimates of the thermodynamics of azotosome self-assembly.

## 5.1 Can Membranes be Operable on Titan?

Whether acrylonitrile can self-assemble into azotosomes depends on whether or not the structure is thermodynamically favoured compared to all other possibilities. Under the frigid temperatures of Titan, the most stable arrangement of most molecules larger than methane is the solid crystal structure. The freezing point of acrylonitrile is 190 K. At 153 K, the crystal structure of acrylonitrile was determined by Yokoyama and Ohashi to be disordered.[105] There are four ordered packings that are consistent with the crystal structure measurements (see Paper II). We compared the electronically most stable crystal structure with the azotosome modelled as a two-dimensional periodic structure. The azotosome structure was built based on the description by Stevenson et al.[103] with the nitrile groups placed in a hexagonal grid. The energy of the structures was evaluated using the Vienna Ab Initio Simulation Package (VASP),[106, 107] a periodic DFT code. We considered thermal effects through phonon calculations on the acrylonitrile crystal structure and the azotosome. Effects of methane solvation were studied by comparing the energy of the azotosome solvated in methane with the non-solvated membrane and solid methane. We also used molecular dynamics to simulate the solvated azotosome to give yet another indication of its kinetic stability.

A summary of the results of Paper II are found in Figure 5.2, where the most stable phase of acrylonitrile $Pna2_1$ is shown and compared to that of the azotosome. The estimate of the relative energy of the azotosome is 8-11 kJ/mol acrylonitrile above the crystal structure. The range in energy arises because the relative energies have been evaluated with different methods for describing dispersion interactions (PBE[23]-D3[97] and vdw-df-cx.[108], see Paper II) The difference in relative energy per monomer is small. However, multiple such building blocks are required to form one mol of membrane. In other words, as more and more molecules are incorporated in the azotosome, the energy separation between the membrane and the crystal structure becomes larger and larger, and consequently the likelihood of forming the higher energy membrane decreases even more. We therefore conclude that the formation of azotosomes, while offering a plausible alternative membrane that is more favored in the seas of Titan than the Earth like ones, are not likely to form.

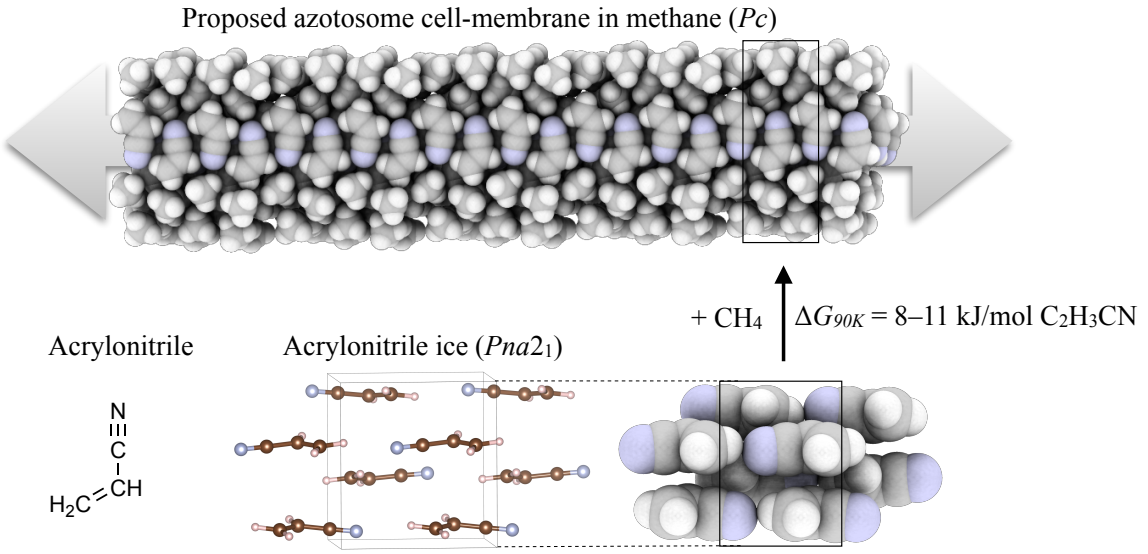


**Figure 5.2** Quantum chemical predictions of membrane stability. Density functional theory calculations predict that the azotosome is not a thermodynamically viable candidate for self-assembly of cell-like membranes on Titan. The necessary building block acrylonitrile will preferentially form the molecular crystal structure, which has a lower Gibbs energy. Crystal symmetries of the considered phases are shown within parenthesis. Figure is reproduced from Sandström and Rahm (Paper II).[109]

## 5.2 Comparing Acrylonitrile Solubility and Critical Azotosome Concentration

The self-assembly of acrylonitrile azotosomes depends on the relative energy of the acrylonitrile in the crystal structure, in the azotosome and in liquid methane. As long as the azotosome is less stable than the crystal structure, the critical concentration for azotosome formation will be larger than the solubility, in other words larger than the maximum concentration of acrylonitrile in solution. To demonstrate this principle, we note that the solubility of acrylonitrile has been estimated theoretically to be approximately $10^{-10}$ M (based on methane molar density of 28 M[110] at 94 K, 1.5 bar and a solubility of $10^{-11}$ mole fractions[111]). The solubility, $K_p$, is related to the relative energy between the solid and solvated molecule, $\Delta G_{solv-solid}$, according to

$$\Delta G_{solv-solid} = -RTlnK_p \tag{5.1}$$

where $R$ is the gas constant and $T$ is the temperature. This corresponds to a $\Delta G_{solv-solid}$ of ~18 kJ/mol. Using our thermodynamical estimate for the energy of the azotosome, the corresponding relative energy of the azotosome compared to the solvated molecule, $\Delta G_{azotosome-solv}$, is -10 - -7 kJ/mol. In analogy to the critical micellar concentration, the critical concentration, $C_{critical}$, for azotosome formation can be found from $\Delta G_{azotosome-solv}$ according to

$$\Delta G_{azotosome-solv} = RTlnC_{critical}. \tag{5.2}$$

With our relative energy estimate, the critical azotosome concentration is $10^{-6}$-$10^{-4}$ M. Comparing Equations (5.1) and (5.2) we see that as long as the azotosome is less stable than the crystal structure, the critical concentration cannot be reached. As there is no available experimental measurement of the solubility, the values of the solvated molecule's relative energy and the critical azotosome concentration that we present here are only approximate and are subject to change with another solubility estimate. However, the requirement of a more stable azotosome in order for azotosome self-assembly to occur is valid for all solubilities. Using the solubility estimate by Stevenson et al. [111] combined with our relative energy of the azotosome, there is at least a four order of magnitude difference between the solubility and the critical azotosome concentration at 94 K.

## 5.3 Conclusions

To conclude, the results from Paper II strongly suggest that membrane formation in hydrocarbon solvent at low temperature is unlikely and challenged by many factors. The kinetic stability of these structures has been confirmed but the stumbling block for their formation lies with the thermodynamics. We can however not rule out that azotosomes formed from another molecule, or at another temperature could be thermodynamically operable. This work is one of the first of its kind where quantum chemistry is used as a tool to evaluate an astrobiology hypothesis. While in this case the results are not in favor of the hypothesis, the study is an example of the potential for quantum chemistry within the field of astrobiology.

# Chapter 6
# Outlook

The aim of this work was to evaluate hypotheses in prebiotic chemistry and astrobiology using quantum chemistry. The formation of iminoacetonitrile, a possible first reactive intermediate in HCN polymerization, was observed in liquid HCN through the mechanism suggested by Orò in 1961.[68] Our best theoretical estimate of the reaction half-life suggest that iminoacetonitrile forms on a slower timescale (several months) than HCN polymers (days). The comparison indicates that the dimerization reaction is a rate-limiting step of the polymerization process if iminoacetonitrile forms as an intermediate. Our comparison with experiments would further improve through characterization of plausible subsequent polymerization steps. To this end, future work will focus in part on investigating the reactivity of iminoacetonitrile.

In paper II, we showed with quantum chemical methods that the spontaneous self-assembly of acrylonitrile azotosomes in Titan's methane lakes is very unlikely. The study was an example of how quantum chemistry can be used to inform and improve on hypotheses in astrobiology that are difficult to test in the lab. The rich chemistry on Titan makes it an especially exciting place where to test hypotheses of extra-terrestrial life. The next mission to Titan, Dragonfly, will focus on the dunes and craters on the surface, and will shed new light on processes occurring in the environment of the cold moon.[112]

# Chapter 7
# Acknowledgement

This research has been carried out at the Division of Chemistry and Biochemistry at Chalmers University of Technology, Sweden, with financial support from Chalmers University of Technology and the Swedish Research Council (grant 2016-04127). The computations were performed on resources at Chalmers Centre for Computational Science and Engineering (C3SE) provided by the Swedish National Infrastructure for Computing (SNIC).

I would like to thank my main supervisor Martin Rahm, and my colleagues at the Division of Chemistry and Biochemistry for a wonderful work environment.

# References


1. Fortney JJ. The Structure of Jupiter, Saturn, and Exoplanets: Key Questions for High-Pressure Experiments. Astrophysics and Space Science. 2007; 307: 279-283.
2. Ferrière KM. The interstellar environment of our galaxy. Reviews of Modern Physics. 2001; 73: 1031-1066.
3. Lindal GF, Wood GE, Hotz HB, Sweetnam DN, Eshleman VR, Tyler GL. The atmosphere of Titan: An analysis of the Voyager 1 radio occultation measurements. Icarus. 1983; 53: 348-363.
4. Krasnopolsky VA. Chemical composition of Titan's atmosphere and ionosphere: Observations and the photochemical model. Icarus. 2014; 236: 83-91.
5. Lavvas P, Yelle RV, Koskinen T et al. Aerosol growth in Titan's ionosphere. Proceedings of the National Academy of Sciences U S A. 2013; 110: 2729-2734, S2729/1.
6. Hörst SM. Titan's atmosphere and climate. Journal of Geophysical Research: Planets. 2017; 122: 432-482.
7. European Space Agency (ESA), ATG medialab. The Formation of Titan's Haze. [Internet] Accessed November 8 2020; Available from: https://www.nasa.gov/mission_pages/cassini/multimedia/pia17240.html
8. Zahnle K, Schaefer L, Fegley B. Earth's Earliest Atmospheres. Cold Spring Harbor Perspectives in Biology. 2010; 2:
9. Lunine JI. Titan as an analog of Earth's past and future. EPJ Web Conf. 2009; 1: 267-274.
10. Mathé C, Vinatier S, Bézard B et al. Seasonal changes in the middle atmosphere of Titan from Cassini/CIRS observations: Temperature and trace species abundance profiles from 2004 to 2017. Icarus Cassini Mission Science Results. 2020; 344: 113547.
11. Cottini V, Nixon CA, Jennings DE et al. Spatial and temporal variations in Titan's surface temperatures from Cassini CIRS observations. Planetary and Space Science Titan Through Time: A Workshop on Titan's Formation, Evolution and Fate. 2012; 60: 62-71.
12. McCord TB, Hansen GB, Buratti BJ et al. Composition of Titan's surface from Cassini VIMS. Planetary and Space Science First Results on Titan from VIMS Observations Onboard the Cassini/huygens Mission/Astrobiology: The Detection of Life in the Solar System. 2006; 54: 1524-1539.
13. Tomasko MG, Archinal B, Becker T et al. Rain, winds and haze during the Huygens probe's descent to Titan's surface. Nature. 2005; 438: 765-778.
14. Voosen P. NASA to fly drone on Titan. Science. 2019; 365: 15.
15. Solomonidou A, Neish C, Coustenis A et al. The chemical composition of impact craters on Titan. A&A. 2020; 641:
16. Stofan ER, Elachi C, Lunine JI et al. The lakes of Titan. Nature. 2007; 445: 61-64.
17. Tokano T, McKay CP, Neubauer FM et al. Methane drizzle on Titan. Nature. 2006; 442: 432-435.
18. Lunine JI, Cable MK, Glein CR, Hörst SMR, M. The Astrobiology of Titan. In: Meadows V, Des Marais DJ, Arney G, Schmidt B, editors. Planetary Astrobiology. Tuscon: University of Arizona; 2020. p. 247-266.
19. Born M, Oppenheimer R. Zur Quantentheorie der Molekeln. Annalen der Physik. 1927; 389: 457-484.
20. Purvis GD, III, Bartlett RJ. A full coupled-cluster singles and doubles model: the inclusion of disconnected triples. J Chem Phys. 1982; 76: 1910-1918.
21. Hohenberg P, Kohn W. Inhomogeneous Electron Gas. Phys Rev B. 1964; 136: 864-871.

22. Kohn W, Sham LJ. Self-Consistent equations including exchange and correlation effects. Phys Rev. 1965; 140: A1133.
23. Perdew JP, Burke K, Ernzerhof M. Generalized gradient approximation made simple. Phys Rev Lett. 1996; 77: 3865-3868.
24. Becke AD. A new mixing of Hartree-Fock and local density-functional theories. J Chem Phys. 1993; 98: 1372-1377.
25. Schwerdtfeger P. The Pseudopotential Approximation in Electronic Structure Theory. ChemPhysChem. 2011; 12: 3143-3155.
26. Bloechl PE. Projector augmented-wave method. Phys Rev B: Condens Matter. 1994; 50: 17953-17979.
27. Togo A, Tanaka I. First principles phonon calculations in materials science. Scr Mater. 2015; 108: 1-5.
28. Tomasi J, Mennucci B, Cammi R. Quantum Mechanical Continuum Solvation Models. Chem Rev. 2005; 105: 2999-3093.
29. Barnett RN, Landman U, Nitzan A, Rajagopal G. Born–Oppenheimer dynamics using density-functional theory: Equilibrium and fragmentation of small sodium clusters. The Journal of Chemical Physics. 1991; 94: 608-616.
30. Tuckerman ME, Martyna GJ. Understanding Modern Molecular Dynamics: Techniques and Applications. The Journal of Physical Chemistry B. 2001; 105: 7598.
31. Bussi G, Donadio D, Parrinello M. Canonical sampling through velocity rescaling. The Journal of Chemical Physics. 2007; 126: 014101.
32. Branduardi D, Gervasio FL, Parrinello M. From A to B in free energy space. The Journal of Chemical Physics. 2007; 126: 054103.
33. Barducci A, Bussi G, Parrinello M. Well-Tempered Metadynamics: A Smoothly Converging and Tunable Free-Energy Method. Physical Review Letters. 2008; 100: 020603.
34. Bolhuis PG, Chandler D, Dellago C, Geissler PL. Transition Path Sampling: Throwing Ropes Over Rough Mountain Passes, in the Dark. Annual Review of Physical Chemistry. 2002; 53: 291-318.
35. Barducci A, Bonomi M, Parrinello M. Metadynamics. WIREs Computational Molecular Science. 2011; 1: 826-843.
36. Pietrucci F, Saitta AM. Formamide reaction network in gas phase and solution via a unified theoretical approach: Toward a reconciliation of different prebiotic scenarios. Proceedings of the National Academy of Sciences USA. 2015; 112: 15030.
37. Torrie GM, Valleau JP. Nonphysical sampling distributions in Monte Carlo free-energy estimation: Umbrella sampling. Journal of Computational Physics. 1977; 23: 187-199.
38. Kertész J, Kondor I, editors. Error estimates on averages of correlated data Advances in Computer Simulation. 1998; Berlin, Heidelberg: Springer Berlin Heidelberg; 1998.
39. Tokunaga AT, Beck SC, Geballe TR, Lacy JH, Serabyn E. The detection of HCN on Jupiter. Icarus. 1981; 48: 283-289.
40. Lellouch E, Romani PN, Rosenqvist J. The vertical Distribution and Origin of HCN in Neptune's Atmosphere. Icarus. 1994; 108: 112-136.
41. Lellouch E, Gurwell M, Butler B et al. Detection of CO and HCN in Pluto's atmosphere with ALMA. Icarus. 2017; 286: 289-307.
42. Marten A, Gautier D, Owen T et al. First Observations of CO and HCN on Neptune and Uranus at Millimeter Wavelengths and Their Implications for Atmospheric Chemistry. The Astrophysical Journal. 1993; 406: 285.
43. Rodgers SD, S.B. C. HNC and HCN in Comets. The Astrophysical Journal Letters. 1998; 501: L227.

44. Tanguy L, Bézard B, Marten A et al. Stratospheric profile of HCN on Titan from millimeter observations. Icarus. 1990; 85: 43-57.
45. Buhl D, Snyder LE. Nature. 1970; 228: 267.
46. Loison J-C, Wakelam V, Hickson KM. The interstellar gas-phase chemistry of HCN and HNC. Monthly Notices of the Royal Astronomical Society. 2014; 443: 398-410.
47. Pau CF, Hehre WJ. Heat of formation of hydrogen isocyanide by ion cyclotron double resonance spectroscopy. Journal of Physical Chemistry. 1982; 86: 321-322.
48. DePrince III AE, Mazziotti DA. Molecular Geometries and Harmonic Frequencies from the Parametric Two-Electron Reduced Density Matrix Method with Application to the HCN ↔ HNC Isomerization. The Journal of Physical Chemistry B. 2008; 112: 16158-16162.
49. Lavvas PP, Coustenis A, Vardavas IM. Coupling photochemistry with haze formation in Titan's atmosphere, Part II: Results and validation with Cassini/Huygens data. Planet Space Sci. 2008; 56: 67-99.
50. Teanby NA, Irwin PGJ, de K, R. et al. Vertical profiles of HCN, HC3N, and C2H2 in Titan's atmosphere derived from Cassini/CIRS data. Icarus. 2007; 186: 364-384.
51. Coustenis A, Schmitt B, Khanna RK, Trotta F. Plausible condensates in Titan's stratosphere from Voyager infrared spectra. Planetary and Space Science. 1999; 47: 1305-1329.
52. Samuelson RE, Smith MD, Achterberg RK, Pearl JC. Cassini CIRS update on stratospheric ices at Titan's winter pole. Icarus. 2007; 189: 63-71.
53. Clark RN, Curchin JM, Barnes JW et al. Detection and mapping of hydrocarbon deposits on Titan. J Geophys Res Planets. 2010; 115: E10005.
54. Panda M, Robinson NC. Kinetics and mechanism for the binding of HCN to cytochrome c oxidase. Biochemistry. 1995; 34: 10009-10018.
55. European Southern Observatory(ESO), NASA. The Galactic Centre and Sagittarius B2. [Internet] 2009. Accessed 6 November 2020; Available from: https://www.eso.org/public/images/eso0924e/
56. NASA, Jet Propulsion Laboratory-Caltech, Space Science Institute. Enhanced-color view of Titan taken by Cassini on Sept. 13, 2017. [Internet] 2017. Accessed November 5, 2020; Available from: https://www.nasa.gov/image-feature/jpl/pia21890/a-last-look-at-titan
57. European Space Agency (ESA). Image of 67P/Churyumov-Gerasimenko shows the diversity of surface structures on the comet's nucleus. [Internet] 2014. Accessed 5 november 2020; Available from: https://www.nasa.gov/jpl/rosetta/comet-surface-variations-20140815/
58. Martiniano HFMC, Costa Cabral BJ. Structure and electronic properties of a strong dipolar liquid: Born-Oppenheimer molecular dynamics of liquid hydrogen cyanide. Chem Phys Lett. 2013; 555: 119-124.
59. Coates GE, Coates JE. Hydrogen Cyanide. Part XIII. The Dielectric Constant of Anhydrous Hydrogen Cyanide. Journal of Chemical Society. 1944; 77-81.
60. Giauque WF, Ruehrwein RA. The Entropy of Hydrogen Cyanide. Heat Capacity, Heat of Vaporization and Vapor Pressure. Hydrogen Bond Polymerization of the Gas in Chains of Indefinite Length. J Am Chem Soc. 1939; 61: 2626-2633.
61. Brandao I, Rivelino R, Fonseca TL, Castro MA. An ab initio study of electric properties of linear (HCN)N and (HNC)N aggregates in gas phase. Chem Phys Lett. 2013; 580: 9-13.
62. Loew GH, Chang S, Berkowitz D. Quantum chemical study of relative reactivities of a series of amines and nitriles: Relevance to prebiotic chemistry. Journal of Molecular Evolution. 1975; 5: 131-152.

63. Dulmage WJL, W. N. The Crystal Structures of Hydrogen Cyanide HCN. Acta cryst. 1951; 4: 330-334.
64. Rahm M, Belanger-Chabot G, Haiges R, Christe KO. Nitryl Cyanide, NCNO2. Angew Chem, Int Ed. 2014; 53: 6893-6897.
65. Miller SL. A Production of Amino Acids under Possible Primitive Earth. Science. 1953; 117 3046: 528-529.
66. Miller SL, Urey HC. Organic Compound Synthesis on the Primitive Earth. Science. 1959; 130: 245-251.
67. Oró J. Synthesis of adenine from ammonium cyanide. Biochemical and Biophysical Research Communications. 1960; 2: 407-412.
68. Oro J. Mechanism of synthesis of adenine from HCN under possible primitive earth conditions. Nature. 1961; 191: 1193-1194.
69. Ruiz-Bermejo M, Zorzano M-P, Osuna-Esteban S. Simple organics and biomonomers identified in HCN polymers: an overview. Life (Basel, Switz). 2013; 3: 421-448.
70. Miyakawa S, James Cleaves H, Miller SL. The Cold Origin of Life: A. Implications Based On The Hydrolytic Stabilities Of Hydrogen Cyanide And Formamide. Origins Life Evol Biosphere. 2002; 32: 195-208.
71. Sutherland JD. The Origin of Life-Out of the Blue. Angew Chem, Int Ed. 2016; 55: 104-121.
72. Marin-Yaseli MR, Moreno M, Briones C, de LFJL, Ruiz-Bermejo M. Experimental conditions affecting the kinetics of aqueous HCN polymerization as revealed by UV-vis spectroscopy. Spectrochim Acta A Mol Biomol Spectrosc. 2017; 191: 389-397.
73. Ruiz-Bermejo M, de LFJL, Carretero-Gonzalez J et al. A Comparative Study on HCN Polymers Synthesized by Polymerization of NH4 CN or Diaminomaleonitrile in Aqueous Media: New Perspectives for Prebiotic Chemistry and Materials Science. Chem Eur J. 2019; 25: 11437 - 11455.
74. Sanchez RA, Ferris JP, Orgel LE. Prebiotic synthesis. II. Synthesis of purine precursors and amino acids from aqueous hydrogen cyanide. J Mol Biol. 1967; 30: 223-253.
75. Ruiz-Bermejo M, de la Fuente JL, Rogero C, Menor-Salvan C, Osuna-Esteban S, Martin-Gago JA. New Insights into the Characterization of 'Insoluble Black HCN Polymers'. Chem Biodiversity. 2012; 9: 25-40.
76. Mas I, de la Fuente JL, Ruiz-Bermejo M. Temperature effect on aqueous NH4CN polymerization: Relationship between kinetic behaviour and structural properties. European Polymer Journal. 2020; 132: 109719.
77. Umemoto K, Takahasi M, Yokota K. Studies on the structure of HCN oligomers. Origins of life and evolution of the biosphere. 1987; 17: 283-293.
78. Mamajanov I, Herzfeld J. HCN polymers characterized by SSNMR: Solid state reaction of crystalline tetramer (diaminomaleonitrile). J Chem Phys. 2009; 130: 134504/1-134504/5.
79. Mozhaev PS, Kichigina GA, Kiryukhin DP, Barkalov IM. Radiation-induced polymerization of hydrogen cyanide. High Energy Chem (Transl of Khim Vys Energ). 1995; 29: 15-18.
80. Khare BN, Sagan C, Thompson WR, Arakawa ET, Meisse C, Tuminello PS. Optical properties of poly-HCN and their astronomical applications. Can J Chem. 1994; 72: 678-694.
81. Maillard J, Hupin S, Carrasco N, Schmitz-Afonso I, Gautier T, Afonso C. Structural elucidation of soluble organic matter: Application to Titan's haze. Icarus. 2020; 340: 113627.

82. He C, Smith MA. A comprehensive NMR structural study of Titan aerosol analogs: Implications for Titan's atmospheric chemistry. Icarus. 2014; 243: 31-38.
83. Nna-Mvondo D, de la Fuente JL, Ruiz-Bermejo M, Khare B, McKay CP. Thermal characterization of Titan's tholins by simultaneous TG-MS, DTA, DSC analysis. Planet Space Sci. 2013; 85: 279-288.
84. Völker T. Polymere Blausäure. Angewandte Chemie. 1960; 72: 379-384.
85. Garbow JR, Schaefer J, Ludicky R, Matthews CN. Detection of secondary amides in hydrogen cyanide polymers by dipolar rotational spin-echo nitrogen-15 NMR. Macromolecules. 1987; 20: 305-309.
86. He C, Lin G, Upton KT, Imanaka H, Smith MA. Structural Investigation of HCN Polymer Isotopomers by Solution-State Multidimensional NMR. J Phys Chem A. 2012; 116: 4751-4759.
87. Mamajanov I, Herzfeld J. HCN polymers characterized by solid state NMR: Chains and sheets formed in the neat liquid. J Chem Phys. 2009; 130: 134503/1-134503/6.
88. Miyakawa S, Cleaves HJ, Miller SL. The Cold Origin of Life: B. Implications Based on Pyrimidines and Purines Produced From Frozen Ammonium Cyanide Solutions. Origins of life and evolution of the biosphere. 2002; 32: 209-218.
89. Coates JE, Harthorne NH. Studies on hydrogen cyanide. Part III. The Freezing Points of Hydrogen Cyanide. Journal of Chemical Society. 1931; 0: 657-665.
90. Sanchez R, Ferris J, Orgel LE. Conditions for Purine Synthesis: Did Prebiotic Synthesis Occur at Low Temperatures. Science. 1966; 153: 72.
91. Ferris JP, Donner DB, Lotz W. Chemical evolution. IX. Mechanism of the oligomerization of hydrogen cyanide and its possible role in the origins of life. Journal of the American Chemical Society. 1972; 94: 6968-6974.
92. Evans RA, Lorencak P, Ha TK, Wentrup C. HCN dimers: iminoacetonitrile and N-cyanomethanimine. J Am Chem Soc. 1991; 113: 7261-7276.
93. Kliss RM, Matthews CN. HCN dimer and chemical evolution. Proc Natl Acad Sci U S A. 1962; 48: 1300-1306.
94. Rivilla VM, Martín-Pintado J, Jiménez-Serra I et al. Abundant Z-cyanomethanimine in the interstellar medium: paving the way to the synthesis of adenine. Monthly Notices of the Royal Astronomical Society: Letters. 2018; 483: L114-L119.
95. Zaleski DP, Seifert NA, Steber AL et al. Detection of E-Cyanomethanimine Toward Sagittarius B2(N) in the Green Bank Telescope Primos Survey. The Astrophysical Journal. 2013; 765: L10.
96. Kikuchi O, Watanabe T, Satoh Y, Inadomi Y. Ab initio GB study of prebiotic synthesis of purine precursors from aqueous hydrogen cyanide: dimerization reaction of HCN in aqueous solution. Journal of Molecular Structure: THEOCHEM. 2000; 507: 53-62.
97. Grimme S, Ehrlich S, Goerigk L. Effect of the damping function in dispersion corrected density functional theory. J Comput Chem. 2011; 32: 1456-1465.
98. Hutter J, Iannuzzi M, Schiffmann F, VandeVondele J. cp2k: atomistic simulations of condensed matter systems. Wiley Interdisciplinary Reviews: Computational Molecular Science. 2014; 4: 15-25.
99. Szostak JW, Bartel DP, Luisi PL. Synthesizing life. Nature. 2001; 409: 387-387.
100. McKay CP, Smith HD. Possibilities for methanogenic life in liquid methane on the surface of Titan. Icarus. 2005; 178: 274-276.
101. Lunine JI. Titan and habitable planets around M-dwarfs. Faraday Discuss. 2010; 147: 405-18; discussion 527.

102. Anslyn EV, Dougherty DA. Modern Physical Organic Chemistry. Sausalito, CA: University Science; 2006
103. Stevenson J, Clancy P, Lunine J. Membrane alternatives in worlds without oxygen: Creation of an azotosome. Sci Adv. 2015; 1: e1400067.
104. Palmer MY, Cordiner MA, Nixon CA et al. ALMA detection and astrobiological potential of vinyl cyanide on Titan. Sci Adv. 2017; 3: e1700022.
105. Yokoyama Y, Ohashi Y. Crystal Structure of Acrylonitrile. Bull Chem Soc Jpn. 1998; 71: 345-348.
106. Kresse G, Furthmueller J. Efficient iterative schemes for ab initio total-energy calculations using a plane-wave basis set. Phys Rev B: Condens Matter. 1996; 54: 11169-11186.
107. Kresse G, Joubert D. From ultrasoft pseudopotentials to the projector augmented-wave method. Phys Rev B: Condens Matter Mater Phys. 1999; 59: 1758-1775.
108. Berland K, Hyldgaard P. Exchange functional that tests the robustness of the plasmon description of the van der Waals density functional. Phys Rev B. 2014; 89: 035412.
109. Sandström H, Rahm M. Can polarity-inverted membranes self-assemble on Titan. Sci Adv. 2020; 6: eaax0272.
110. Setzmann U, Wagner W. A New Equation of State and Tables of Thermodynamic Properties for Methane Covering the Range from the Melting Line to 625 K at Pressures up to 100 MPa. Journal of Physical and Chemical Reference Data. 1991; 20: 1061-1155.
111. Stevenson JM, Fouad WA, Shalloway D et al. Solvation of nitrogen compounds in Titan's seas, precipitates, and atmosphere. Icarus. 2015; 256: 1-12.
112. Turtle EP, Trainer MG, Barnes JW et al. Dragonfly: In Situ Exploration of Titan's Organic Chemistry and Habitability. 50th Lunar and Planetary Science Conference. 2019; Abstract #2888.